



Thermal Oxidation of PEPA-terminated Polyimide

Xiaochen Li, Masahiko Miyauchi, Carlos González, and Steven R. Nutt*

M.C. Gill Composites Center, Department of Chemical Engineering and Materials Science, University of Southern California, 3651 Watt Way VHE-602, Los Angeles, CA 90089-0241, USA

* E-mail: nutt@usc.edu

Abstract: The thermal oxidative stability of a 4-phenylethynyl phthalic anhydride (PEPA) endcapped polyimide (PI) was investigated. A surface reaction layer formed due to oxidization during thermal aging and grew in thickness with increasing aging time. Analysis of the surface layer revealed a partial loss of aromatic ring, ether linkage, and imide linkage in the aged polymer. The partial loss of the imide linkage and ether linkage in the surface layer was corroborated by the observed release of carbon monoxide and carbon dioxide reaction products. The oxidized layer exhibited discoloration and an increase in glass transition temperature. The surface discoloration was attributed to the formation of the conjugated unsaturated or aromatic carbonyl groups and/or the charge transfer complex. Interior regions of the oxidized samples were largely unaffected, except for a more compact molecular configuration. Compared with aging at high temperatures (288°C, 316°C), aging at 204°C produced similar chemical changes in the cured polymer, albeit with a low degradation rate. The oxidative stability of the imide polymer surpassed that of conventional nadic-endcapped PIs due to the greater intrinsic thermal stability of the PEPA endcap. The unusual oxidative stability of the PI, combined with superior mechanical properties, warrant consideration as a composite matrix for future applications in high-temperature service conditions.



Key words: Phenylethynyl phthalic anhydride, polyimide, thermal oxidative stability, degradation, discoloration, Fourier transform infrared, X-ray photoelectron spectroscopy, composites.

1. INTRODUCTION

Oxidative reactions in polyimides (PIs) can potentially cause problems that include cracking, brittleness, chemical changes, all of which can compromise retention of mechanical properties. In this work, we explore and report the thermal oxidative stability of a new PI and associated composites. In particular, we identify chemical changes associated with anticipated high-temperature service conditions in oxidizing ambient.

PIs are widely used in high-temperature composite applications because of the high glass transition temperatures (T_g s) and thermal stability. However, PIs generally suffer from poor processability, cracking induced by thermal shock, and thermal oxidation. Phenylethynyl phthalic anhydride (PEPA)-terminated PIs have been developed to address such limitations, and these polymers generally offer wider process windows and improved heat resistance, although they are not immune to oxidation and thermal shock damage. A new class of PEPA-terminated pyromellitic dianhydride (PMDA)-type PI, denoted TriA-X,1 has been developed in an attempt to address the limitations of brittleness and poor processability associated with most PIs. The TriA-X PI is derived from PMDA and 2-phenyl-4,4'-diaminodiphenyl ether (p-ODA). The pendent phenyl group of p-ODA restricts molecular interaction and decreases the rotational flexibility of the chain.² The distinctive chemical structure of the polymer imparts a reduced elastic modulus during heating (from 109 Pa to 107 Pa before and after glass transition), which facilitates processing of carbon fiber composites.²

Chemical changes occurring during PI oxidation are not fully understood, due in part to the complexity of the oxidation reaction. Incomplete understanding of oxidation mechanisms limits efforts to redesign and optimize the molecular structure of PI. Thus, for the TriA-X PI, understanding the thermal oxidative stability



is necessary to evaluate performance as a high-temperature material. The objective of this study is to determine the mechanisms of thermal oxidative degradation of the PI TriA-X. We investigate the degradation effects of thermal oxidation, including weight loss, formation of an oxidized layer, and microcrack formation. The reaction products generated during thermal oxidation are also investigated to provide insights into the physical changes.

Reports on the oxidation behavior of PI formulations have shown that an oxidized surface layer typically forms. For example, one PI long used in the aerospace industry is PMR-15 (PMR stands for polymerized monomeric reactant). During thermal oxidation of PMR-15,³ a reaction occurs that results in evolution of three distinct regions—an oxidized shell, an active reaction zone, and a nonoxidized core.⁴ Analysis of the oxidized surface layer of PMR-15 with norbornenyl-endcap showed that the nadic endcap skeleton was virtually undetectable.⁵ The methylene moiety oxidized to ketone, causing shrinkage and stiffening of the chain. Other possible degradation pathways have been proposed that involve degradation of the nadic endcap moiety and the methylene dianiline moiety.⁶ However, the mechanism of weight loss has not been identified, and the possible thermal degradation of the nonoxidized core was not investigated. In related work, the oxidation behavior of PI composites was investigated. For example, Xie et al. studied the oxidative stability of carbon fiber (CF)-PI composites (AFR 700B/T650-35) using thermogravimetric analysis–mass spectroscopy (TGA-MS).⁷ By analyzing gaseous species generated during heating, they proposed multiple possible chain breakdown sites, mostly related to the end norbornene group, the end aniline group, the –CF₃–C–CF₃–, and the imide ring. The use of TG-MS provided real-time detection of release of degradation products. However, aging mechanisms in long-term high-temperature applications may differ from the reaction mechanisms detected during the more aggressive conditions of accelerated pyrolysis in TGA.

The present PI (TriA-X) features a distinctive molecular structure that is likely to impart oxidation mechanisms and kinetics unlike nadic endcap PIs. In particular, the PEPA endcap of TriA-X does not contain carbon with sp³ hybridization, unlike the norbornenyl-endcap often employed in PIs. After cross-linking, the



bond dissociation energy (BDE) of the alkenyl phenyl bond is approximately 452 kJ mol⁻¹,⁸ rendering the endcap resistant to pyrolysis and release of free radicals. For the backbone, the (TriA-X) molecule also exhibits greater heat resistance than PMR-15 by virtue of the replacement of the methylene bridge in the diamine with the biphenyl ester group. The oxidation-susceptible bond in the TriA-X backbone is most likely the imide bond, which possesses a low BDE (approximately 270 kJ mol⁻¹).⁹ Thus, due to the distinctive backbone structure and endcap species, TriA-X PI is expected to exhibit oxidation behavior unlike other PIs. These differences may lead to distinct oxidation kinetics, a different oxidization growth mechanism, and different effects on mechanical properties.¹⁰

In this work, we identify reaction mechanisms that occur during the thermal oxidation of the PEPA-terminated PI (TriA-X). We also show that the PEPA-terminated PI molecule exhibits superior thermal stability compared with nadic endcapped PI (PMR-15), exhibiting less rapid weight loss and an absence of aging-induced cracks. The thermal stability stems from the intrinsic stability of the PEPA endcap, which exceeds that of the PI backbone and the nadic endcap. Unlike PMR-15, a single distinct oxidized layer forms during thermal oxidation, and the reaction responsible is attributed to breakage and rearrangement of the imide ring, ether group, and the PEPA endcap. Aging at moderate temperature was also conducted to compare with aging at higher temperature typically employed in accelerated aging studies, and the oxidation mechanism was consistent in both regimes.

2. EXPERIMENTS

2.1. Material Preparation and Aging Condition

The chemicals PMDA (Tokyo Kasei Kogyo, Japan), PEPA (Manac, Japan), and p-ODA (Wakayama Seika Kogyo, Japan) were obtained from Kaneka Corporation. The monomer mixture was prepared by mixing the chemicals in a hot ethanol solution, followed by vacuum



drying. After preliminary screening, the ratio of PMDA, p-ODA, and PEPA was chosen to be 7:8:2 (degree of polymerization, $n = 7$) and confirmed by nuclear magnetic resonance measurements.

The PI panel used for the aging study was produced using a hot press with a metal mold. The monomer mixture was first converted to oligomer by heating to 280°C for 60 min. The resulting oligomer was ground to fine powder and placed in a steel mold 3 mm deep. The oligomer was heated to 370°C for 150 min to achieve cross-linking. Reaction scheme and molecular structure are shown in [Figure 1](#).

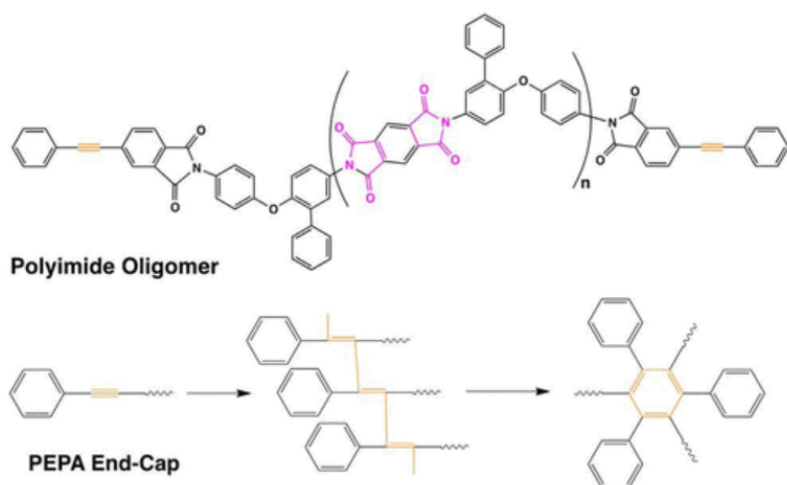


Figure 1. Molecular structure of the TriA-X oligomer and reaction scheme of cross-linking of PEPA end cap. PEPA: phenylethynyl phthalic anhydride.

Prior to oxidation, all samples were preheated to 200°C for 1 h to remove moisture. Oxidative aging treatments up to 2000 h were performed in an air-circulated oven set to 204, 288, and 316°C to accelerate aging. The latter aging temperatures were chosen for comparison with reported data on PMR-15, while 204°C was chosen to approximate anticipated service



temperatures. Aging treatments were interrupted periodically to remove samples for measurements.

2.2. Weight Change

Ten PI panels were cut to $100 \times 10 \times 3 \text{ mm}^3$ coupons for weight measurements. After preheating, the dimensions of the coupons were measured and repeated 10 times to determine the total surface area, and the initial weight prior to aging was measured using a balance with 0.01 mg accuracy. Coupons were placed in an air-circulated oven for thermal oxidative aging and removed periodically for weight measurements. Samples were placed in a desiccator to prevent moisture absorption during cooling. The weight change per unit area was calculated for each of the 10 coupons. Thin polished sections (0.3–0.4 mm) were prepared for microscopic observation using transmitted light (VHX-5000, Keyence, Osaka, Japan).

2.3. Dynamic Mechanical Analysis

The T_g was determined by conducting dynamic mechanical analysis tests (DMA 2980; TA Instruments, New Castle, USA). A dynamic ramp of 5°C min^{-1} was performed from 30°C to 500°C . Three groups of samples were tested: (1) unaged neat PI (TriA-X) samples, (2) neat PI samples ($3 \times 10 \times 30 \text{ mm}^3$) aged in an air-circulated oven for 20, 50, 100, 250, 500, 1000, 1500, and 2000 h, and (3) neat PI samples aged in an air-circulated oven for 20, 50, 100, 250, 500, 1000, 1500, and 2000 h with each exposed surface polished to at least 0.5 mm. To measure the thickness of the oxidized layer, polished sections of unaged and aged samples were prepared and inspected using light microscopy.

2.4. Nanoindentation



Indentation tests on the aged specimens were carried out using a Hysitron TI 950 TriboIndenter (Minneapolis, MN, USA) equipped with a diamond Berkovich tip. Tests were performed at room temperature using the continuous strain rate method, with $d\varepsilon/dt = (dh/dt)/h = 0.075 \text{ s}^{-1}$, where h is the penetration depth of the indenter in the polymer substrate. The maximum penetration depth was $h = 2 \text{ }\mu\text{m}$ and the load was $P_{\text{max}} = 5000 \text{ }\mu\text{N}$. Special care was taken to avoid viscous effects on the load–displacement curve by performing a hold-step while maintaining constant load and measuring the required properties during a subsequent unload. For each material sample, at least 10 indentations were carried out in different locations of the specimen. The material apparent hardness H and the elastic modulus E were determined from the load–displacement curve in the unloading cycle after the hold period using geometrical area of the Berkovich indenter and the elastic compliance. Thus, artifacts due to polymer pileup surrounding the tip masking the true contact area were avoided in the analysis.

2.5. Fourier Transform Infrared

Attenuated total reflection–Fourier transform infrared (FTIR; Nicolet 4700) was employed to obtain IR spectra from aged samples. Sections were prepared from (a) the thermally oxidized surface and (b) the interior of the PI sample, and both were polished to films less than $100 \text{ }\mu\text{m}$ thick. Wavenumbers from 4000 cm^{-1} to 400 cm^{-1} were collected, and 64 scans were performed for each sample. Coupled TGA-FTIR experiments were performed under a nitrogen (N_2) atmosphere using a heating rate of $10^\circ\text{C min}^{-1}$ up to 850°C to detect and identify reaction products as they evolved. Scanning FTIR (Hyperion, Bruker, Billerica, USA) was conducted on the cross section of the aged TriA-X with reflective light. IR spectra were acquired from the surface to the interior every $30 \text{ }\mu\text{m}$. The typical light spot diameter was $20\text{--}50 \text{ }\mu\text{m}$.



2.6. X-ray Photoelectron Spectroscopy

X-ray photoelectron spectroscopy (XPS, Kratos Axis Ultra DLD, Manchester, UK) was used to determine the composition of PI films before and after thermo-oxidative aging. Thin-film polished sections were prepared from the exposed surface and the sample interior. The oxidized surface and the interior were analyzed using an aluminum anode under 10^{-9} – 10^{-8} torr vacuum with sampling depth 2–10 nm. For each sample, a survey spectrum was acquired to obtain overall composition, followed by three high-resolution scans for carbon, oxygen, and nitrogen. For O 1s, the range for binding energy was chosen as 550–525 eV, and for C 1s, 310–215 eV. Fifteen sweeps were conducted for each range.

3. RESULTS AND DISCUSSION

3.1. Weight Loss

The weight loss of the PI with aging time at 316 and 288°C was shown in [Figure 2](#). The rate of weight loss during aging, as shown in [Table 1](#), at 316°C ($0.739 \text{ mg} \times \text{mm}^2 \times \text{h}^{-1}$) was approximately 4.2× greater than the weight loss rate for aging at 288°C ($0.176 \text{ mg} \times \text{mm}^2 \times \text{h}^{-1}$). Both rates were much less than the rate of weight loss values reported previously for PMR-15 (approximately $0.35 \text{ mg} \times \text{mm}^2 \times \text{h}^{-1}$ for 288°C,¹¹ approximately $8.5 \text{ mg} \times \text{mm}^2 \times \text{h}^{-1}$ for 316°C¹²), indicating greater thermal stability.

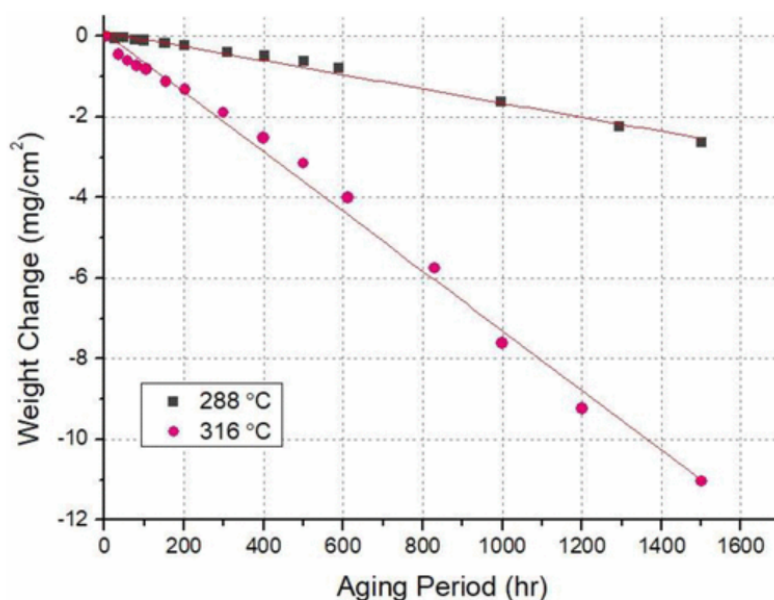


Figure 2. Weight loss per unit area of TriA-X during isothermal oxidative degradation at 288 and 316°C.

Table 1. Weight loss rate of PMR-15 and TriA-X neat polymer at different temperature.

Aging temperature	Weight loss rate	
	PMR-15 (mg × mm ² × h ⁻¹)	TriA-X (mg × mm ² × h ⁻¹)
288°C	~0.35 ¹¹	0.176
316°C	~8.5 ¹²	0.739

PMR: polymerized monomeric reactant.

The surprisingly low rate of weight loss observed can be attributed primarily to the absence of surface and bulk cracks in the PI here (TriA-X). Cracking and crazing are commonly reported during thermal oxidation and thermal cycling of PIs and PI composites.^{11–14} In addition, voids reportedly appear in oxidized layers of PMR-15 aged at 288 and 316°C.¹⁵ Microcracks and voids exacerbate surface reactions in PIs, providing pathways for accelerated ingress of oxygen,



increasing the rate of weight loss. Thus, during thermal oxidation of conventional PI (e.g. PMR-15, 316°C in air), the weight loss shows a power-law dependence on aging time (exponent = 1.63), which is attributed to an increase in exposed surface area caused by crazing, cracking, and pitting.¹² However, during oxidation at 288 and 316°C, the PI here (TriA-X) shows a quasi-linear weight loss relationship with time, and no cracking was observed at the surface or in the bulk. Note that, although weight loss for 316°C data appear to be linear, close inspection shows an apparent acceleration of mass loss rate near 400 h, which would indicate a breakdown of a passive protection.

The endcap of the PI molecule affects the rate of weight loss during oxidation. PIs with norbornenyl endcaps (such as PMR-15) undergo more rapid weight loss compared with PIs sharing the same backbone.⁶ Meador et al. provided evidence that the most rapid large initial loss is due to degradation of the nadic-endcap.⁶ In contrast, for nadic-endcapped PIs, the initial rate of weight loss decreases as the relative amount of nadic decreases.¹⁶ Note that PMR-15, where $n = 2$, is expected to have greater cross-linking density than TriA-X ($n = 7$). For TriA-X, $n = 7$ was studied due to its balance of mechanical and thermal performances. Many factors could account for the lower weight loss rate, such as absence of microcrack and lower cross-linking density. It also can be attributed to the greater thermal stability of the PEPA endcap than the nadic end cap. Degradation of the TriA-X backbone and PEPA endcap is discussed in subsequent sections.

Cross sections of the unaged and thermally oxidized TriA-X PI samples after aging at different conditions are shown in [Figure 3](#). Aged at 288 and 316°C, the surface of the aged polymer shows discoloration when illuminated with transmitted light, and the discoloration is attributed to the generation and accumulation of highly conjugated groups or other chromophores.¹⁷ For aging at



204°C, no distinct discolored layer was observed even after 2000 h. The oxidized layer thickness in the sample aged at 316°C is less than the layer thickness produced by aging at 288°C, which is a typical diffusion/reaction result.¹⁸ The oxidized layer that grows rapidly during high aging temperature retards further diffusion of oxygen. Aging at 204°C did not produce a detectable oxidized layer, possibly because the critical oxidized layer thickness (L_c)¹⁸ at this temperature exceeded half the sample thickness ($0.5 \times L$), and/or because the process at this temperature is limited more by the reaction rate than by diffusion.

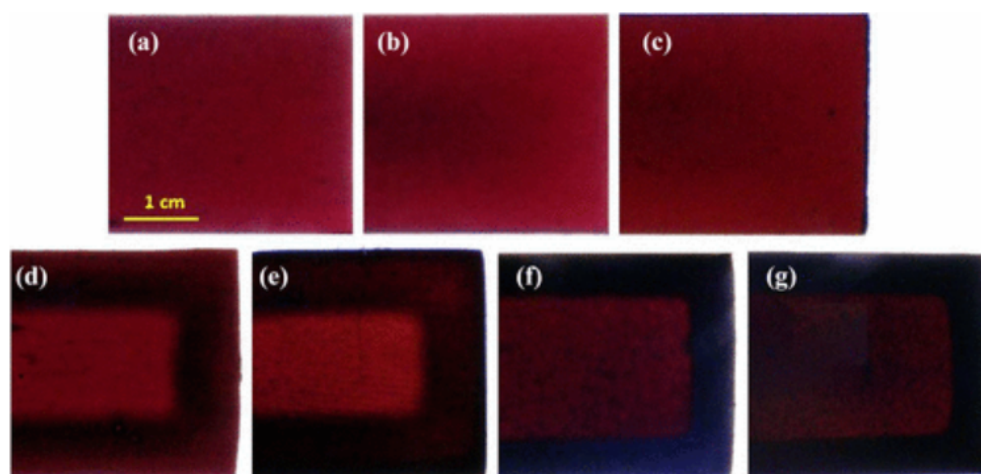


Figure 3. Cross section of TriA neat polymer (a) unaged; (b) 204°C, 700 h; (c) 204°C, 2000 h; (d) 288°C, 700 h; (e) 288°C, 1500 h; (f) 316°C, 700 h; and (g) 316°C, 1500 h.

The absence of cracks in the aged polymer is largely responsible for the lower rate of weight loss observed. In the following sections, the discolored region will be referred to as the oxidized layer, while the translucent interior region will be referred to simply as the interior. The entire sample (interior plus oxidized layer) will be referred to as the bulk sample.

3.2. Thermal Analysis



DMA experiments were performed to measure the T_g (via $\tan(\delta)$) for unaged PI and PI thermally oxidized at 288°C for different times, and the results are shown in [Figure 4](#). In general, T_g increased with aging time ([Figure 4\(a\)](#)), and similar increases in T_g have been reported after thermal oxidation of PMR-15.¹³ In [Figure 4\(a\)](#), at 500 h, the $\tan(\delta)$ peak became broader and less symmetric with aging time and temperature, while the peak centroid shifted to higher temperature. After further aging for 1000 and 2000 h, the $\tan(\delta)$ peak exhibited a shoulder at the lower temperature flank, and longer aging times caused apparent peak separation, with a second peak developing near 325°C.

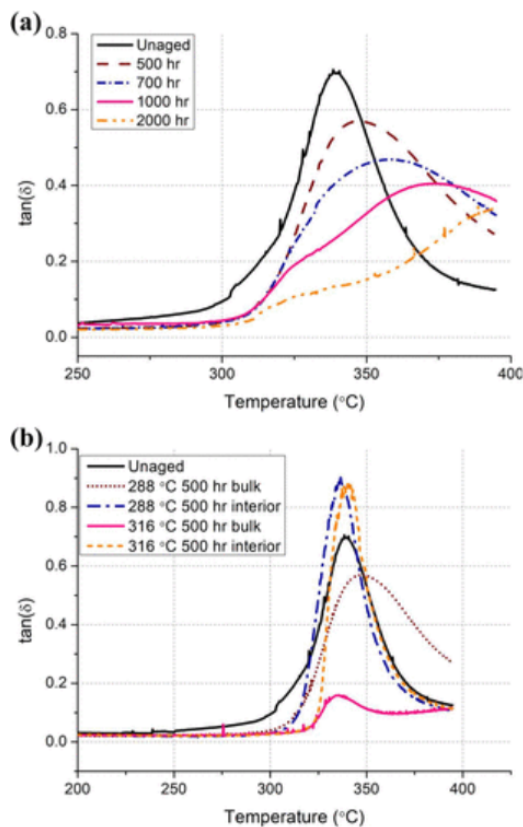


Figure 4. (a) $\tan(\delta)$ of TriA-X during aging at 288°C and (b) $\tan(\delta)$ of bulk and interior TriA-X after aging.



Two possible explanations were considered for the peak separation observed in Figure 4(a)—(1) β relaxation of the oxidized PI and (2) formation of a second phase during aging. To distinguish between these two possibilities, DMA samples were prepared from the aged bulk polymer and from the aged interior (with oxidized layer removed), and the results are shown in Figure 4(b).

As shown in Figure 4(b), removing the oxidized surface layer also removed the broad high-temperature $\tan(\delta)$ peak ($>350^{\circ}\text{C}$). Thus, the low-temperature peak (at approximately 330°C) must originate from the interior of the sample, while the broad peak at approximately 350°C corresponds to the discolored oxidized layer. Furthermore, the interior and the oxidized layer exhibit different thermal mechanical behaviors. No obvious change of the value of T_g for the interior was observed after aging, indicating that the chemical structure here was largely unaffected by aging (see Figure 4(b)). The author also observed an increase in G' , which indicates the interior undergoes physical aging such as reduction in free-volume and decrease of mobility. In contrast, a notable change is apparent the oxidized layer. In Figure 4(b), the broadening of the α relaxation peak at high temperature indicates the growth of a thicker oxidized layer with different chemical structures, wider molecular weight distribution, or more compact packing. In the FTIR section, we attribute the stronger intra/intermolecular interactions between the polymer chains to the loss of pendant phenyl groups of p-ODA¹ and/or the generation of oxidative products.

3.3. Nanoindentation Measurements

The apparent hardness H (indentation load divided by imprint projected area) and elastic modulus E of the unaged polymer, aged polymer on the surface exposed to aging, and aged polymer interior are shown in Figure 5. The larger standard deviation obtained for the aged surface tests is



attributed to the sample preparation procedure, which left initial roughness on the surface. Nevertheless, both the elastic modulus and the hardness increased in tests carried out on the specimen surface, while the specimen interior showed almost no change with aging time, as shown in [Figure 5\(a\) and \(b\)](#). The trends for surface and interior hardness converge to a single value as aging time decreases, corresponding to the unaged polymer. Note that the elastic modulus of the unaged TriA-X (≈ 4.70 GPa) as measured by indentation is remarkably similar to the nanoindentation elastic modulus of PMR-15 (≈ 4.72 GPa).¹⁹

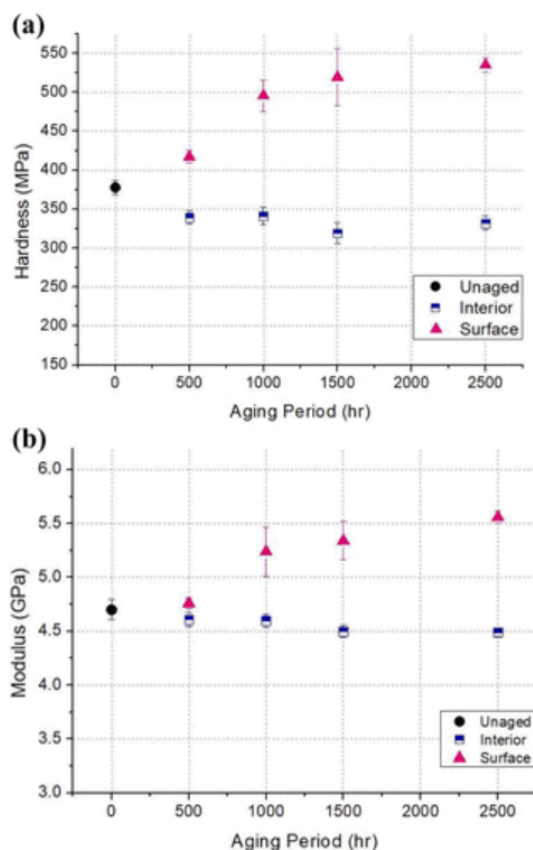


Figure 5. (a) Nanoindentation hardness of the unaged and aged resin surface and interior and (b) nanoindentation modulus of the unaged and aged resin surface and interior.



After aging, both hardness and modulus on the surface increased. This increase indicates the generation of a hard oxidized surface layer on the polymer. The surface layer features strong intermolecular interactions that increase with aging time. In contrast, both hardness and modulus remain nearly constant for interior regions of the sample, with only a slight decrease. With thermal oxidative aging of PMR-15 and other thermosets, an increase in modulus of the oxidized layer is commonly observed.^{15,19} In PMR-15, the average elastic modulus in the oxidized region is insensitive to aging time.¹⁹ However, for TriA-X, a continuous increase in hardness with aging time was observed, ([Figure 5](#)), indicating a continuous change in the chemical composition of the surface. To clarify the reaction that occurs during thermal oxidation, FTIR and XPS were used to analyze the chemical composition.

3.4. FTIR Analysis

Chemical changes in PIs during thermal oxidation can be identified using FTIR spectroscopy of aged samples. In previous research, chemical changes during oxidative degradation and thermal cycling of PIs with norbornenyl endcaps were monitored by tracking changes in FTIR spectra. Based on the results, investigators proposed conversion of methylene from the methylenedianiline moiety to a carbonyl group.⁶ Degradation of the O=C–N moiety in the imide ring and degradation of C=C in the unreacted nadic endcap were also proposed as possible degradation reactions.⁶ However, the present PI (TriA-X) lacks a methylene group in the monomer, and the endcap has no C–C and C=C bonds, and thus must follow a different pathway to oxidative degradation. FTIR spectra acquired from samples of unaged and aged PI, both surface and interior, showed the progressive change in chemistry during thermal oxidation ([Figures 6 and 7](#)). Spectra from the polymer surface ([Figure 6\(a\)](#)) show a decrease in a set of peaks (arrows) relative to the



spectra of the aged polymer interior, which are nearly unchanged. Figure 6(b) shows that the spectrum after aging at 288°C shows less change compared with aging at 316°C for the same time, while the spectrum after aging at 204°C shows only a slight decrease at 1218 and 695 cm^{-1} (compare Figures 6(a) and 5(b)).

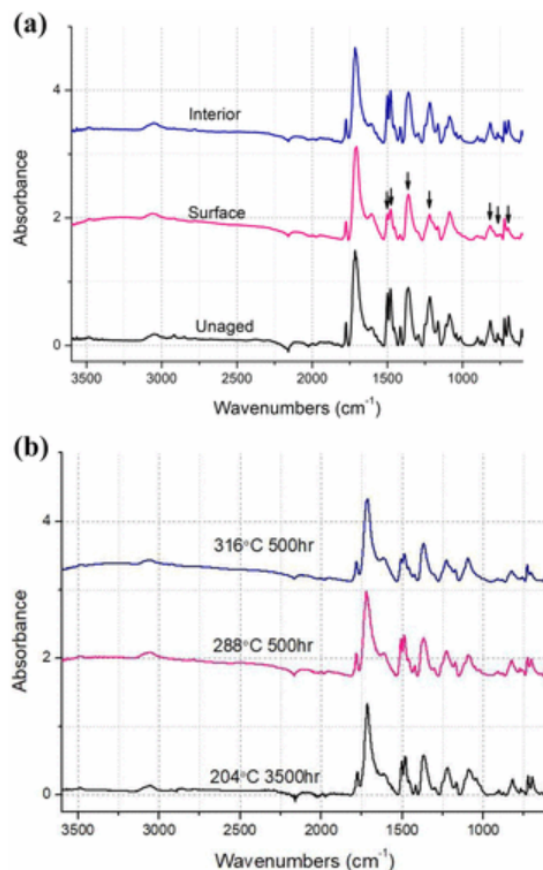


Figure 6. (a) FTIR spectra of fresh TriA-X versus 316°C 500-h aged resin surface and interior and (b) FTIR spectra of TriA-X aged at different temperatures and times. FTIR: Fourier transform infrared.

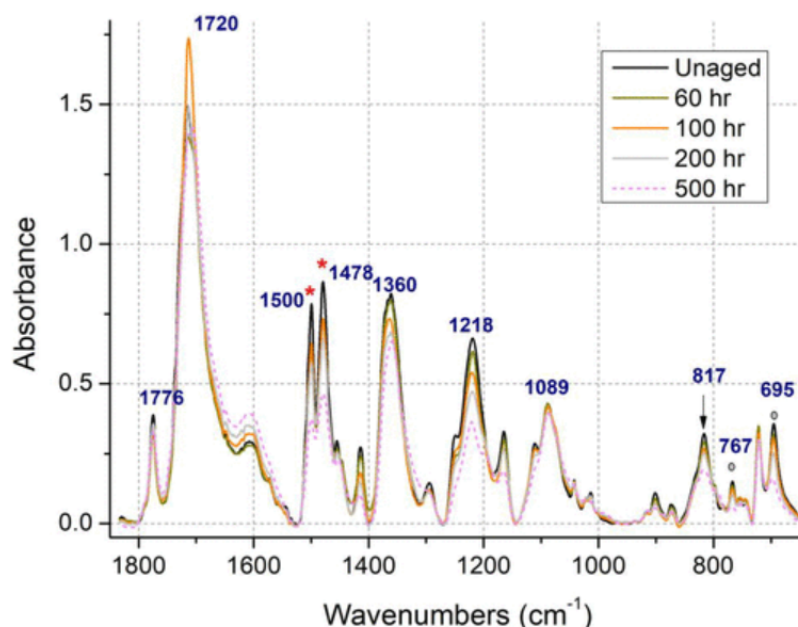


Figure 7. FTIR spectra of fresh TriA-X versus resin surface after aging at 316°C for different times. FTIR: Fourier transform infrared.

FTIR spectra from the unaged surface show bands generated from the imide ring, appearing at 1776, 1720, 1360, and 721 cm^{-1} (Figure 7). Bands at 1776 and 1720 cm^{-1} correspond to the in-phase and out-of-phase stretch of the imide carbonyl. After oxidation, FTIR spectra show that the peak at 1720 cm^{-1} overlapped the carbonyl peak of the oxidation product. Meador et al.⁶ and Hay et al.²⁰ assigned the band at 721 cm^{-1} (719 cm^{-1}) (which decreased with aging) to the out-of-plane bending of the C=C on the unreacted nadic endcap. However, we assigned this peak to deviational vibration of the imide ring because of its absence in the spectrum from monomer powder, and the proportional relationship with peaks at 1776 and 1360 cm^{-1} . The observed slight decrease in amplitude of the imide ring-related peaks reflects the instability of the imide group during aging at 288 and 316°C.



Figure 7 also shows the effects of aging time on FTIR spectra acquired from the oxidized surface. With increasing aging time, there is a slight but steady decrease in band amplitude relative to the aromatic ring (Ar). Skeletal vibration of the benzene ring resulted in strong bands at 1500 and 1478 cm^{-1} (labeled with red *) and these bands decreased with increasing oxidation time. C–H bending peaks of the monosubstituted aromatic ring were observed at 767 and 695 cm^{-1} (circle mark). The mono-Ar peak comes from both the PEPA endcap and p-ODA. The band at 817 cm^{-1} (arrow) was assigned to the C–H bending of the para-disubstituted aromatic ring. Some of the weak overtone bands of the aromatic ring skeletal vibration were obscured by the strong C=O bands in the region of 1600–1800 cm^{-1} . The peak at 1218 cm^{-1} (asterisk) was assigned to the phase stretch of Ar–O–Ar.^{21,22} Compared with the imide band at 721 cm^{-1} , bands at 1218, 817, 767, and 695 cm^{-1} show clear decreases during oxidation, indicating lower thermal oxidative stability of the Ar–Ar, Ar–O–Ar, and Ar–N bonds compared to the imide ring at 316°C. After protracted aging at lower temperature (204°C for 3500 h), a slight decrease in relative intensity of Ar–O–Ar bond and mono-Ar peak was observed, which may come from the loss of PEPA endcap or p-ODA. Thus, at higher aging temperatures (288 and 316°C), the p-ODA and PEPA endcap showed lower stability compared with imide-related groups.

Loss of the monosubstituted aromatic ring on the p-ODA moiety can account for the observed discoloration of the surface layer. Before aging, this benzene ring caused steric hindrance to reduce formation of inter/intrachain charge transfer complex (CTC) between nitrogen (electron donor) and the carbonyl group (electron acceptor).²³ By removing this benzene pendant from the backbone, the inter/intrachain packing becomes stronger by the formation of a more rigid CTC, accounting



for the darker color of the aged surface layer. The more rigid packing also accounts for the increase in hardness and modulus of the aged surface layer.

Oxidation products were identified from specific peaks which developed after aging at 316°C (Figure 7). For example, the peak at 1607 cm^{-1} was assigned to the stretching of the conjugated C=O group generated by oxidation.⁶ Bands at 1218 and 1089 cm^{-1} were attributed to stretching of the C–O in the Ar–O–Ar moiety. However, instead of decreasing proportionally with the band at 1218 cm^{-1} , the band at 1089 cm^{-1} increased and broadened slightly, then finally became greater in amplitude than the band at 1218 cm^{-1} . The increase and broadening of the strong peak at 1089 cm^{-1} was attributed to the generation of alkoxy groups from the ester or acid of oxidation products, which overlapped with the ether C–O peaks in the spectrum. The bands at 1196 and 1607 cm^{-1} were assigned to acyl stretching and C=O bending, leading to the conclusion that the oxidation products were primarily unsaturated esters. Ketone is proposed as another possible oxidation product, due to the appearance of the strong band near the 1710 cm^{-1} region.

FTIR spectra generally do not provide clear indications of post-curing during thermal oxidation. In the TriA-X PI, there was no sp^1 C–H in the alkynes group of the endcap before aging, nor was there a sp^2 C–H in the cross-linked endcap. The bands of $\text{C}\equiv\text{C}$ and $\text{C}=\text{C}$ overlapped with carbon dioxide (CO_2) peaks and the existing strong peaks of benzene. Consequently, changes in chemical composition of the endcap, such as post-cross-linking and degradation, were not apparent. The interior of the aged samples yielded spectra much like those of PMR-15,⁶ with no sign of cross-linking (because of the absence of C–H bands). Bands for nitriles and alkynes, which were detected as intermediates during the ultraviolet laser-induced decomposition and pyrolysis of Kapton,²⁴ were not observed after thermal oxidation of TriA-X.



Scanning FTIR revealed progressive degradation from the polymer surface to the interior, as shown in [Figure 8](#), which plots the concentration of chemical groups as a function of subsurface distance. To compare degradation of different chemical groups, the intensities of five peaks—1720 cm^{-1} ($\text{C}=\text{O}$), 1360 cm^{-1} ($\text{C}-\text{N}$ of the imide ring), 1218 cm^{-1} (ether linkage), 695 cm^{-1} (mono-Ar), and 817 cm^{-1} (para-Ar)—were measured and compared with the intensities of the peaks of the interior. [Figure 9](#) shows that the monosubstituted aromatic ring which comes from the PEPA endcap and ether linkage has the lowest stability, followed by the ether linkage with the next lowest stability. The intensity for the $\text{C}=\text{O}$ group decreased less than the $\text{C}-\text{N}$ group because of the generation of oxidative product, which also contained $\text{C}=\text{O}$ groups. The similarity of the curves for the para-aromatic ring and the $\text{C}-\text{N}$ peak indicates that these two groups degraded almost simultaneously. The oxidized layer for this sample (aged at 288°C for 700 h) was approximately 800 μm thick, and this value is consistent with that of the discolored region. The correlation indicates that the discoloration can be attributed to progressive chemical degradation (which is accompanied by increases in hardness and T_g).

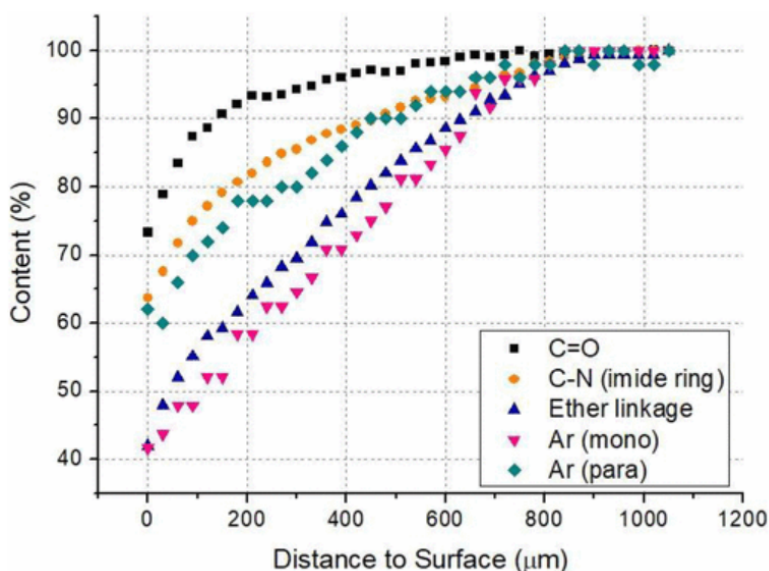




Figure 8. Content of chemical groups of the 288°C 700-h aged resin oxidized layer

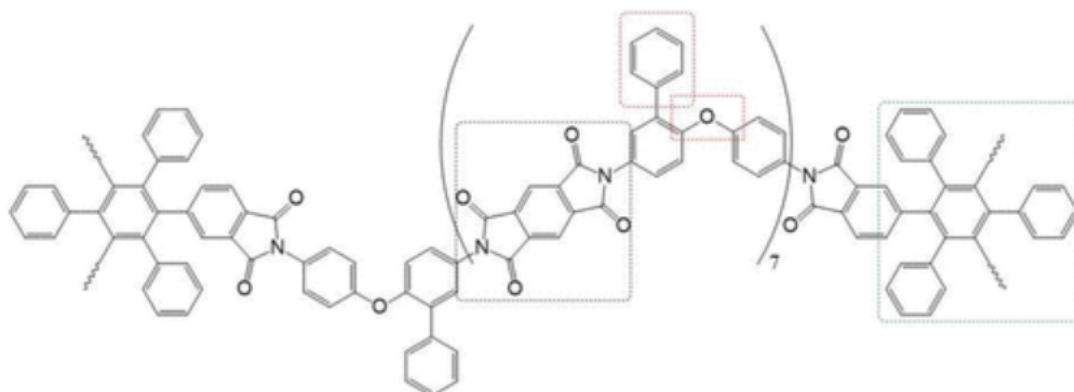


Figure 9. Instable groups of TriA-X in thermal oxidative environment.

FTIR analysis shows the instable chemical groups in the polymer chain and endcap, shown in [Figure 10](#). Fang et al.²⁵ proposed multiple phenylethynyl reactions and further reactions for the curing of polyene and aromatic ring structures for the PEPA endcap. To further assess the thermal stability of the chemical bonds in TriA-X, dynamic TGA was performed, and the volatiles were analyzed by FTIR ([Figure 10\(a\)](#)). The intensity curve shows that the PI started to decompose under N₂ atmosphere at approximately 500°C and reached the highest decomposition rate at approximately 576°C. The FTIR spectra from volatiles released at 545 and 625°C during dynamic ramp represent the early and later stages of decomposition, and it is discussed next.

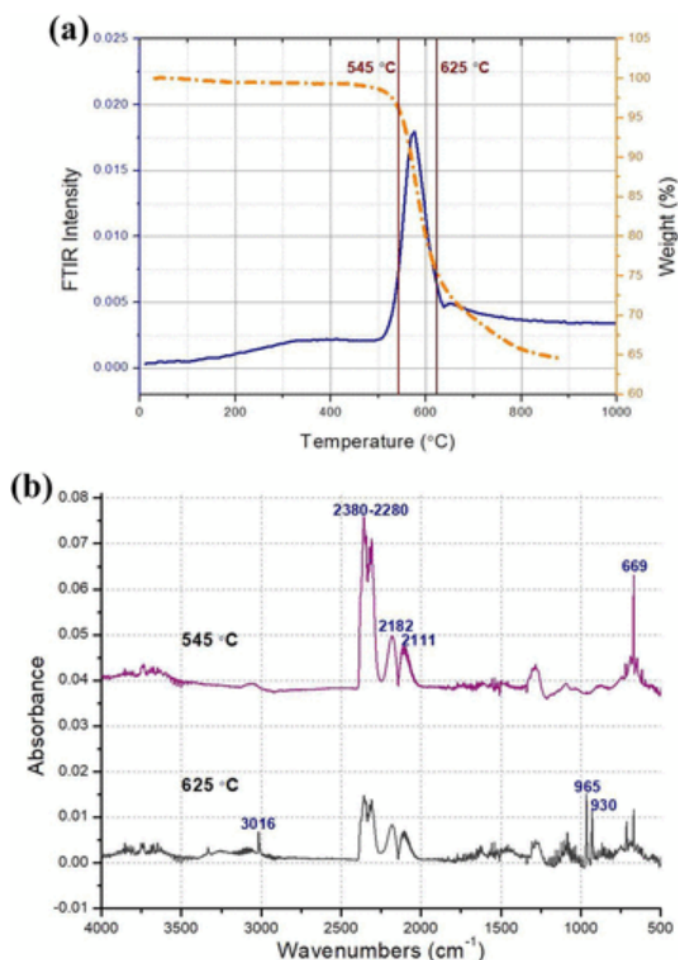


Figure 10. (a) FTIR intensity of the released volatile and weight loss percentage during the TGA dynamic ramp and (b) FTIR spectra of the volatile released at 545 and 625 °C. FTIR: Fourier transform infrared; TGA: thermogravimetric analysis.

The primary volatiles generated at 545 °C were identified as carbon monoxide (CO; 2182 cm⁻¹, 2111 cm⁻¹) and CO₂ (2380–2280 cm⁻¹, 669 cm⁻¹, red curve in [Figure 10\(b\)](#)). During pyrolysis in the absence of O₂, CO and CO₂ are generated from the decomposition and rearrangement of the imide ring and ether linkage of the p-ODA. In contrast, the spectrum acquired at 625 °C exhibited bands associated with unsaturated alkyl groups, including bands at 3016 cm⁻¹ from sp² C–H stretching, and at 965, 930, and 714 cm⁻¹ from sp² C–H bending (black curve



in Figure 10(b)). Alkene is the primary released species, although the broad band at 3110–2990 cm^{-1} indicates the possible existence of an aromatic ring. The fluctuating peaks in the high wave number region ($>3500 \text{ cm}^{-1}$) reflect constant generation of H_2O molecules from the beginning of the ramp, initially as absorbed moisture, then later as a decomposition product in the high-temperature region. The small peak at 3333 cm^{-1} , can be assigned to small amounts of amines, particularly $\text{C}_6\text{H}_5\text{--NH}_2$ and $\text{CH}_2\text{=CH--NH}_2$.

Analysis of the TGA-FTIR data reveals that under N_2 atmosphere, the ether linkage and imide ring on the polymer backbone have lower thermal stability, which is consistent with the scanning FTIR spectra and with previous reports on pyrolysis and carbonization of Kapton^{24,26} and AFR 700B.⁷ The generation of $\text{C}_6\text{H}_5\text{--NH}_2$ and $\text{CH}_2\text{=CH--NH}_2$ stems from the decomposition of $\text{--Ar--CO--N(CO)--Ar--}$ and --Ar--O--Ar-- bonds, which have relatively low BDEs and thus lower thermal stability. The BDE for Ar--O--Ar is $329.7 \text{ kJ mol}^{-1}$,²⁷ while the BDEs for Ar--Ar and Ar--vinyl are approximately $450\text{--}460 \text{ kJ mol}^{-1}$.⁸ Thus, in the absence of O_2 , bonds with lower BDE have higher tendency to break.

The small amounts of alkene and aromatic groups detected by IR are possible degradation products of the endcap, but may also arise from decomposition of benzene rings within p-ODA of the backbone. Even if the alkene and aromatic groups arise from decomposition of the PEPA endcap, the IR intensity of these species is much weaker than the IR intensity of CO_2 and CO , especially in the early stage of weight loss. These observations indicate that in the absence of O_2 , the thermal stability of the PEPA endcap is greater than that of the backbone. However, for nadic-endcapped PIs, the endcap-related species (cyclopentadiene and methanol (CH_3OH)) exhibit greater relative intensity compared to backbone-generated species.⁷ Thus, the TGA-FTIR results



indicate that in O₂-free environments, PEPA endcap has greater thermal oxidative stability than both the PI backbone and the conventional norbornenyl endcap.

3.5. Surface XPS Analysis

To clarify the change in chemical composition during oxidation and to identify possible nonvolatile oxidation products, XPS spectra of C 1s and O 1s were acquired from the unaged polymer, the aged surface, and the aged interior of the TriA-X polymer. In evaluating the XPS spectra, it is useful to consider the ratio of the total area of C 1s over the total area of O 1s (C/O ratio). Using this metric, and considering the effects of oxidation at 316°C for 1000 h, the C/O ratio decreased from 1.43 to 1.10 in spectra from the sample interior. In contrast, in spectra from the oxidized layer, the C/O ratio was 0.99 after oxidation. The decrease in C/O ratio reflects the relative increase in the amount of O during oxidation, as well as the loss of C-related groups.

To understand the changes in binding energy of C 1s, five constituent peaks were separated and plotted, as shown in [Figure 11\(a\)](#). The first of these peaks (peak 1), the broad peak at 284.6 eV, includes (a) the sp² carbon from the alkene groups of the cross-linked endcap, (b) aromatic rings that are not attached to an imide ring, and (c) aromatic carbon of the p-ODA moiety, not directly connected with N or O.^{26,28-30} The second peak (peak 2), at 285.2 eV, arises from (a) carbon atoms shared by the imide ring and the aromatic ring on the endcap, (b) from the C–N bond, and (c) the unsubstituted C in the PMDA aromatic ring.³¹ The third peak (285.7 eV, peak 3) corresponds to the aromatic carbon connected with the imide ring in the backbone. This carbon has an approximately 0.5-eV shift compared to the aromatic carbon connecting with the imide ring in the endcap because of the stronger conjugation effect of the additional imide ring.³¹ This peak also corresponds to the secondary carbonyl carbon from the oxidation product. The fourth peak (286.4



eV, peak 4) corresponds to the C–O carbon of the ether linkage or to alkoxy carbon from the oxidation product. Finally, the peak at 288.6 eV (peak 5) corresponds to the carbonyl carbon from the imide ring.^{29,31}

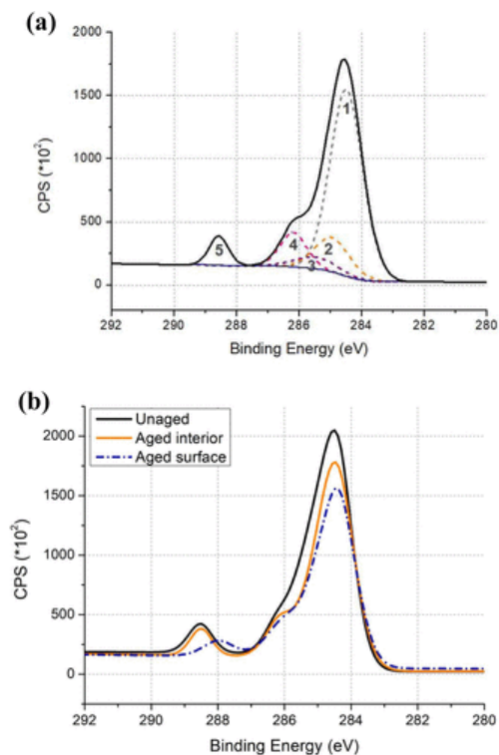


Figure 11. Peak separation for C 1s of the (a) aged interior and (b) C 1s of fresh TriA X and 316 °C 1000 hr aged resin surface and interior.

As shown in Figure 11(b), XPS spectra from the oxidized surface showed distinct differences from the interior. In particular, the shift of the carbonyl peak from 288.6 eV to 288.2 eV reflects consumption of imide rings and generation of oxidation products on the polymer surface. The binding energy at 288.2 eV points to ketone, aldehyde, and amine as possible oxidation products and reduces the possibility of acid (usually this has a binding energy approximately 289.3 eV). The decrease in amplitude of the peak at 285.2 eV also indicates degradation of the imide ring. The increase in the amplitude of the 285.7 eV peak is attributed to



overlap of the secondary C 1s for ketone or aldehyde (approximately 285.4 eV), both possible oxidation products.³¹ Combined with the IR analysis of nonvolatile oxidation products, ketone emerges as the most likely oxidation product. In particular, the carbonyl group, conjugated with an aromatic ring, alkene group, and other unsaturated groups on the polymer chain, constitutes the chromophore for discoloration of the oxidized surface layer.³² The C 1s spectrum from the aged sample interior shows much less differences compared with spectra from the aged surface, as indicated in [Table 2](#). In the sample interior, the peak from the carbonyl carbon of the imide ring (at 288.6 eV) remains constant in integrated intensity, an indication of the stability of the imide group ([Figure 11\(b\)](#)). The relative decrease in amplitude of 285.2 and 285.7 eV compared with the sp² carbon (284.6 eV) may reflect a shift of binding energy due to the formation of a CTC.

Table 2. Area percentage of peaks for C 1s and O 1s of unaged and 316 °C 1000-h aged TriA-X.

Binding Energy (eV)		C 1s					O 1s	
		284.6	285.2	285.7	286.4	288.6	531.5	532.9
Area percentage (%)	Theoretical	52.6	14.7	12.0	6.9	13.8	66.7	33.3
	Unaged	55.9	20.5	7.9	9.2	6.5	72.4	27.6
	Aged interior	65.86	12.9	5.3	9.9	6.1	69.1	30.9
	Aged surface	65.4	7.9	9.0	11.9	5.8 (288.2 eV)	94.1	6.0

Spectra from the aged surface show that the O 1s peak separated into two peaks ([Figure 12\(a\)](#)). The first peak (531.5 eV) is carbonyl, while the second (532.9 eV) is O in the ether group. In [Figure 12\(b\)](#), the total O content increased after aging, and thus both peaks increased in intensity. The relative amplitude of the 532.9 eV peak for the aged interior increased slightly. However, due to the large peak width of O 1s, the binding energy of C–O with a large group of functional groups overlaps in this range, preventing identification of the specific functionality.³¹ On the aged surface, aromatic ether bonds were broken, and C=O became the major species (approximately 94%) resulting from generation of aromatic carbonyl or alkene



carbonyl. These species may have formed the conjugated chromophore in the oxidized layer according to the second discoloration mechanism described earlier.

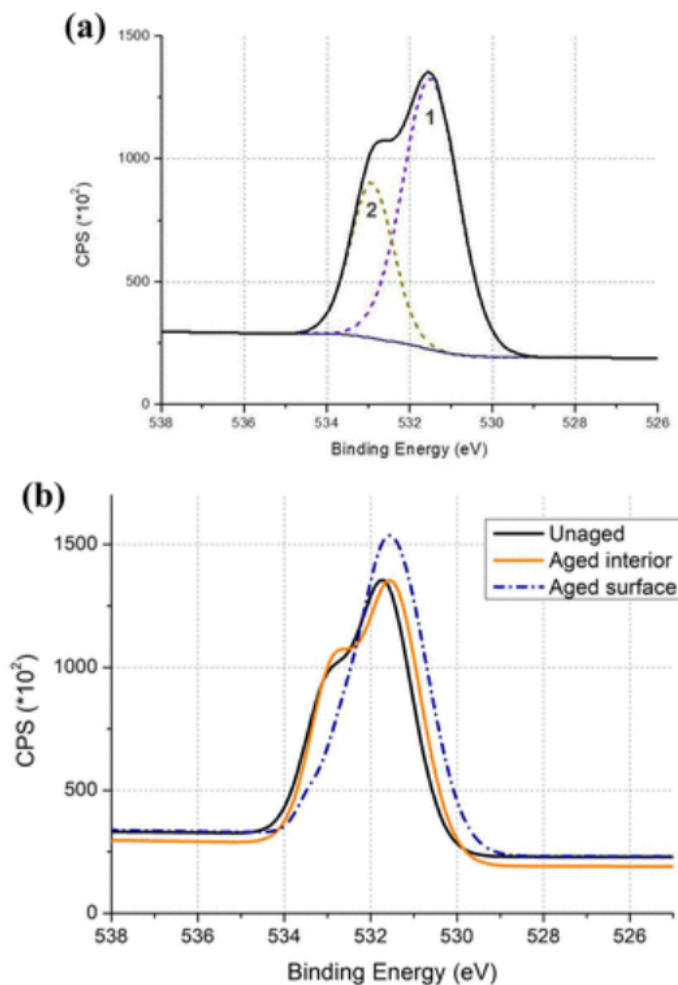


Figure 12. Peak separation for O 1s of the (a) aged interior b) O 1s of fresh TriA X and 316°C 1000 hr aged resin surface and interior.

4. CONCLUSIONS

The thermal oxidation study of TriA-X PI provides understanding of molecular-level reaction mechanisms, such as the degradation of ether moiety and the endcap. During thermal oxidative aging of TriA-X at high temperatures, the PEPA endcap and p-ODA moiety is less stable than the



imide ring. PEPA endcap, which is relatively stable under N₂ atmosphere, were largely affected by the existence of O₂. This provides useful insight to guide further PI development and modification of PIs. Discoloration of the oxidized layer resulted from chemical degradation was observed and investigated. The rigid oxidized surface layer, comprised of unsaturated conjugated ketone chromophore, showed higher hardness and T_g .

The reactions and kinetics at service temperatures may very well differ from those observed at the higher temperatures typically used for accelerated aging studies. Thus, there is an inherent risk in drawing conclusions from accelerated aging experiments. From the present investigation, aging kinetics accelerated with aging temperature, although the chemical changes that occurred during aging at 288 and 316°C aged were unchanged. Aging at 204°C, closer to anticipated service temperatures, shows a much slower but similar oxidation reaction and mechanism.

TriA-X exhibits greater resistance to thermal oxidation than the nadic-endcapped PI, PMR-15, with less weight loss and no cracking. The thermal stability of TriA-X derives from the intrinsic stability of the PEPA endcap relative to the nadic endcap, both in inert and oxidative conditions. These features, coupled with the unusually high ductility of TriA-X, indicate potential to expand the property space for high-temperature polymers, affording greater flexibility to designers of composite parts for high-temperature service. The noncrystalline molecular structure¹ and PEPA endcap are likely to be preferred in future PI polymer development. Furthermore, the principles used to design TriA-X formulations also can be applied to guide development of other high-performance polymers, such as bismaleimides and cyanate ester resin, to increase thermal stability and ductility.

Acknowledgements: The authors would like to thank Kaneka Corporation for their support.



Declaration of Conflicting Interests: The author(s) declared no potential conflicts of interest with respect to the research, authorship, and/or publication of this article

Funding: The author(s) disclosed receipt of the following financial support for the research, authorship, and/or publication of this article: The author received financial support from Kaneka Corporation for the research, authorship, and/or publication of this article.

References:

1. Miyauchi, M, Kazama, K, Sawaguchi, T. Dynamic tensile properties of a novel Kapton-type asymmetric polyimide derived from 2-phenyl-4,4'-diaminodiphenyl ether. *Polym J* 2011; 43(10): 866–868.
2. Miyauchi, M, Ishida, Y, Ogasawara, T. Novel phenylethynyl-terminated PMDA-type polyimides based on KAPTON backbone structures derived from 2-phenyl-4,4'-diaminodiphenyl ether. *Polym J* 2012; 44(9): 959–965.
3. Tandon, GP, Pochiraju, KV, Schoeppner, GA. Modeling of oxidative development in PMR-15 resin. *Polym Degrad Stab* 2006; 91(8): 1861–1869.
4. Tandon, G, Pochiraju, K, Schoeppner, GA. Thermo-oxidative behavior of high-temperature PMR-15 resin and composites. *Mater Sci Eng A* 2008; 498(1–2):
5. Madhukar, MS, Bowles, KJ, Papadopoulos, DS. Thermo-oxidative stability and fiber surface modification effects on the inplane shear properties of graphite PMR-15 composites. *J Compos Mater* 1995; 31(6): 596–618.
6. Meador, MAB, Lowell, CE, Cavono, PJ. On the oxidative degradation of nadic endcapped polyimides: I. Effect of thermocycling on weight loss and crack formation. *High Perform Polym* 1996; 8(3): 363–379.
7. Xie, W, Heltsley, R, Xinhua, C, Study of stability of high-temperature polyimides using TG/MS technique. *J App Polym Sci* 2002; 83(6): 1219–1227.
8. Sanderson, RT . Chemical bonds and bond energy. Academic Press, 1971.
9. Frimer, AA, Cavano, PJ, Alston, WB. New high temperature polyimides based on [5]helicene dianhydride. *High Perform Polym* 1994; 7(1): 93–104.
10. Zhang, Y, Miyauchi, M, Steven, N. Structure and properties of a phenylethynyl-terminated PMDA-type asymmetric polyimide. *High Perform Polym* 2018. DOI: 10.1177/0954008318762592
11. Bowles, KJ, Papadopoulos, SD, Inghram, LL. Longtime durability of PMR-15 matrix at 204, 260, 288, and 316 C. NASA/TM 2001; 2001: 210602.
12. Bowles, KJ, Nowak, G. Thermo-oxidative stability studies of Celion 6000/PMR-15 unidirectional composites, PMR-15, and Celion 6000 fiber. *J Compos Mater* 1988; 22(10): 966–985.
13. Bowles, KJ, Roberts, GD, Kamvouris, JE. Long-term isothermal aging effects on carbon fabric-reinforced PMR–15 composites: compression strength. In: Memorandum, NT (ed) 1995.
14. Kenneth, JB, Douglas, J, Leonhardt, T. Isothermal aging effect on PMR-15 resin. NASA Tech Memo 1992; 24(2):105648.

Please cite the article as: Li, X., Miyauchi, M., González, C., & Nutt, S. “**Thermal oxidation of PEPA-terminated polyimide.**” *High Performance Polymers*, 31[6] (2019), 707–718. DOI: 10.1177/0954008318787852



15. Lu, YC, Tandon, GP, Putthanarat, S. Nanoindentation strain rate sensitivity of thermo-oxidized PMR-15 polyimide. *J Mater Sci* 2009; 44(8): 2119–2127.
16. Mary, ABM, Christopher, JJ, Paul, JC. Oxidative degradation of nadic-end-capped polyimides. 2. Evidence for reactions occurring at high temperatures. *Macromolecules* 1997; 30: 3215–3223.
17. Kim, MH, Byun, DJ, Discoloration mechanism of polymer surface in contact with air–water interface. *J Indus Engi Chem* 2013; 19(3): 920–925.
18. Colin, X, Marais, C, Verdu, J. A new method for predicting the thermal oxidation of thermoset matrices application to an amine crosslinked epoxy. *Polym Test* 2001; 20(7): 795–803.
19. Putthanarat, S, Tandon, GP. Influence of aging temperature, time, and environment on thermo-oxidative behavior of PMR-15: nanomechanical characterization. *J Mater Sci* 2008; 43(20): 6714–6723.
20. Hay, JN, Boyle, JD, Parker, SF. Polymerization of N-phenylnadimide: a model for the crosslinking of PMR-15 polyimide. *Polymer* 1989; 30(6): 1032–1040.
21. Huang, WX, Wunder, SL. FTIR investigation of cross-linking and isomerization reactions of acetylene-terminated polyimide and polyisoimide oligomers. *J Polym Sci B Polym Phys* 1994; 32: 2005–2017.
22. Jin, Y, Zeng, G, Danyang, ZHU., Analysis of structure and imidization of poly (amic acid) using FTIR spectroscopy. *Chin J Appl Chem* 2010; 28(03): 285–262.
23. Liu, Y, Zhang, Y, Lan, QI, High-performance functional polyimides containing rigid nonplanar conjugated triphenylethylene moieties. *Chem Mater* 2012; 24(6): 1212–1222.
24. Ortelli, E, Geiger, F, Lippert, T. Pyrolysis of Kapton in air an in situ drift study. *Appl Spect* 2001; 55(4): 412–419.
25. Fang, X, Xie, XQ, Simone, CD. A solid-state ^{13}C NMR study of the cure of ^{13}C -labeled phenylethynyl end-capped polyimides. *Macromolecules* 2000; 33(5): 1671–1681.
26. Konno, H, Nakaiishi, T, Inagaki, M. State analysis of nitrogen in carbon film derived from polyimide Kapton. *Carbon* 1996; 35(9): 669–674.
27. Scheppingen, WV, Dorrestijn, E, Arends, I. Carbon–oxygen bond strength in diphenyl ether and phenyl vinyl ether_ an experimental and computational study. *J. Phys Chem* 1997; 101(30): 5404–5411.
28. Zeng, DW, Yung, KC, Xie, CS. XPS investigation of the chemical characteristics of Kapton films ablated by a pulsed TEA CO_2 laser. *Surf Coat Technol* 2002; 153(2–3): 210–216.
29. Zeng, DW, Yung, KC. Near-threshold ultraviolet-laser ablation of Kapton film investigated by x-ray photoelectron spectroscopy. *J Mater Res* 2011; 18(1): 53–59.
30. Adhi, KP, Owings, RL. Chemical modifications in femtosecond ultraviolet (248 nm) excimer laser radiation-processed polyimide. *Appl Sur Sci* 2004; 225(1–4): 324–331.
31. Briggs, D. Surface analysis of polymers by XPS and static SIMS. Cambridge: Cambridge University Press, 1998.
32. Li, R, Hu, X. Study on discoloration mechanism of polyamide 6 during thermo-oxidative degradation. *Polym Degrad Stab* 1998; 62: 523–528.